Full Paper

Propellants, Explosives, Pyrotechnics

DOI: 10.1002/prep.201300023

Optical Measurement of Peak Air Shock Pressures Following Explosions

Kevin L. McNesby,*[a] Matthew M. Biss,[a] Richard A. Benjamin,[a] and Ronnie A. Thompson[a]

Abstract: High speed video and streak camera imaging are used to measure peak pressures for explosions of spherical charges of the high explosive C-4 (92% trimethylenetrinitramine, $C_3H_6N_6O_6$). The technique measures the velocity of the air shock produced by the detonation of the explosive charges, converts this velocity to a Mach number, and uses the Mach number to determine a peak shock pressure. Peak pressure measurements are reported from a few millimeters to approximately one meter from the charge surface. Optical peak pressure measurements are compared to peak pressures measured using piezoelectric pressure transducers, and to peak pressure measurements estimated using the blast computer code CONWEP. A discussion of accuracy of peak pressures determined optically is provided.

Keywords: Shock pressure · Optical measurement · Explosions · Near field

1 Introduction

The explosive near field for a detonating high explosive is poorly defined. Most often, the explosive near field is given as covering the distance from the charge center of mass to a distance of many charge initial diameters (typically less than 30), and/or covering the time from $t=0$ to the time when the leading shock separates from the detonation product gases, or in more strict regimes, covering the time from $t=0$ to the time when the detonation product gases reach a fixed composition "freeze out" prior to mixing with ambient air [1,2,3].

This region is often overlooked from an experimental point of view because the destructive nature of the environment in the explosive near field makes measurement difficult. Specifically, peak pressure and impulse measurements in the explosive near field are expensive and often suffer from poor repeatibility because of gauge thermal effects, high intensity light exposure, acceleration/strain, ionization products of the explosion, and the tendency for transducer-type gauges to exhibit degradation in performance with repeated exposure to high blast loadings [4,5].

However, experience indicates that the most important information available from stand-off measurements regarding blast performance of explosives is available exclusively in the near field. Since virtually all explosives exhibit some degree of non-ideality [6], the rate of detonation product expansion, temperature, and finite rate chemistry that occurs in the explosive near field determines all effects demonstrated downrange. Any ability to tailor energy delivery on target, to alter explosive impulse, peak shock, and thermal effect is determined by the chemistry that occurs in the near field. This effect is most important for metallized explosives. The release of energy by metallized explosives, and how this energy release may alter the chemical makeup of detonation product gases has a significant effect on energy deposition on target [7,8]. This paper describes one aspect of quantifying the peak shock pressure in the explosive near field.

2 Background

Figure 1 shows a sequence of laser-illuminated shadowgraphs illustrating the evolution of the explosive near field for a 2 kg cylindrical charge of TNT (trinitrotoluene, $C_6H_2(NO_2)_3CH_3$) [1,9]. In this Figure the near field is defined (somewhat arbitrarily, see above) as the time from detonation to the time when the shock leaves the detonation products, shown in Figure 1 as the fourth image from top, labelled as occurring for this test at 391 microseconds after initiation. For many explosives, it is during this time that chemical reactions (mostly anaerobic), occurring within the detonation product gases, can influence the leading shock. Therefore, it is during this time that chemical tuning of the explosive for post-detonation performance must occur. For example, Figure 2 shows a thermochemcial calculation [3] of detonation product gas distribution for a TNT/Al mixture (80:20 by weight), where the Al has been made inert, or fully reactive. The significance here is that early Al participation in the near field chemistry of the detonation product gases alters their makeup, relative to the case of addition of non-reactive Al. Figure 2 shows that the most significant

[a] *K. L. McNesby, M. M. Biss, R. A. Benjamin, R. A. Thompson*
U.S. Army Research Laboratory
Aberdeen Proving Ground, MD 21005-5066, USA
**e-mail: mcnesby@arl.army.mil*

Figure 1. The evolution of the explosive near field.

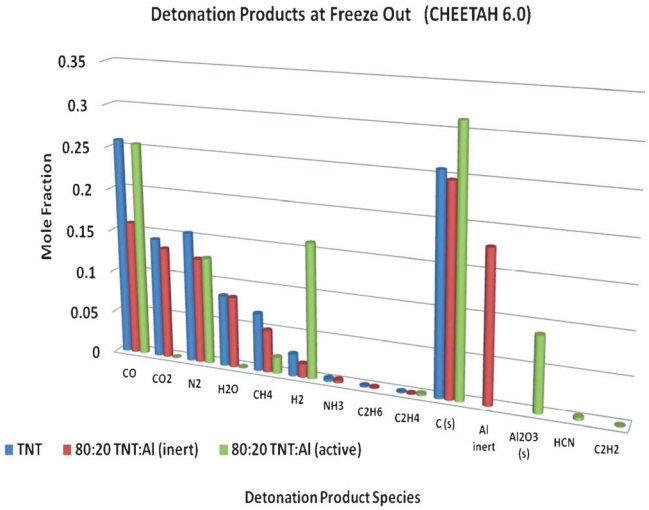

Figure 2. A thermochemical calculation of detonation product gases for a TNT/Al composite explosive – varying Al reactivity.

change due to early Al reactivity is increased H_2 gas in the near field detonation product gases. It has been shown previously that addition of H_2 gas to near field detonation product gases can have a significant effect upon afterburn ignition delay times [7]. The implication being that afterburning times can be tuned to bring detonation product afterburning into proximity of the leading shock, influencing brisance, explosive impulse on target, and enhancing combustion of some non-gaseous detonation products (e.g., for TNT, solid C)[3].

3 Approach

As described above, real tuning of explosives for post-detonation performance will ideally measure output power in the explosive near field. The approach used in what follows concentrates on measurements of the peak shock pressures in real time for exploding, center detonated, 450 g spheres of Composition C-4 (92% trimethylenetrinitramine, RDX, $C_3H_6N_6O_6$, milspec). Figure 3 shows a sequence of high speed framing camera images (2.5 million frames per second (Mfps), 300 nanosecond (nsec) exposure duration) of center detonated C-4 spheres measured using a Cordin Co. Model 570 digital framing camera. A thermochemical calculation [3] indicates that detonation product gas species cease to change in composition when the detonation product gases for C-4 have expanded to approximately twice their initial volume. For the four frames shown in Figure 3, the change in volume is approximately a factor of 19. The approach used here relies on an analysis of high speed images of the type shown in Figure 3, obtained with a framing camera and with streak camera techniques, to measure optically in one test shot the peak shock pressures of exploding C-4 in the near field.

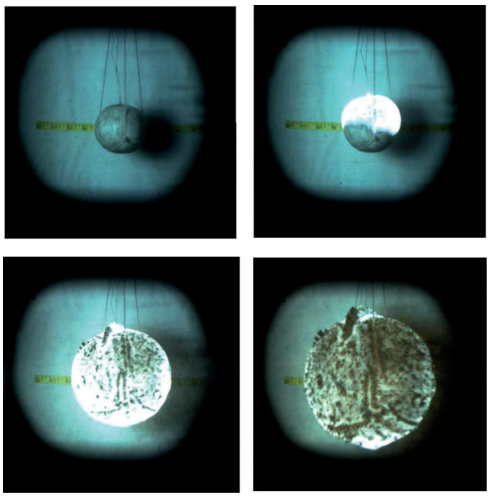

Figure 3. Several images (300 ns exp.) of the explosive near field for 450 g C-4 sphere.

The method of determining shock peak pressures from shock velocities in air is based upon Rankine-Hugoniot theory and may be found in texts on the topic [10]. The equations used here are developed using normal (planar) shocks, but are a reasonable approximation for the spherical shocks produced by the C-4 explosions because of the narrow thickness of the shock front [6,10]. Figure 4 is a schematic of a gas travelling through a stationary shock front. In this model, supersonic gas at ambient pressure p_x at flow velocity u_x enters normal to the shock plane. At the shock plane the gas is decelerated to velocity u_y and compressed to pressure p_y. According to Rankine-Hugoniot theory the shock overpressure, P, is given by Equation (1):

$$P = [(7\,M_x^2 - 1)/6]p_x \qquad (1)$$

Where M_x is the Mach number corresponding to the flow velocity of gas (air) entering the shock plane [10]. The approach employed here is to assume the leading shock is at the surface of the expanding detonation product gases [1]. High speed imaging (framing and streak cameras) is used

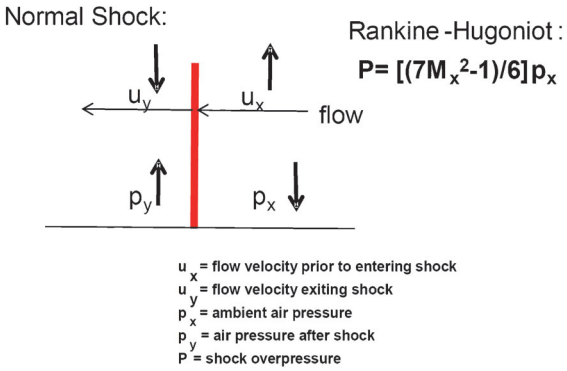

Figure 4. Shock overpressure calculation schematic.

to measure the position of the edge of the detonation product gases, and to measure shock velocities, convert the measured shock velocities to Mach number, and use Equation (1) to calculate peak shock overpressures. This approach has been previously employed by ARL [1] to measure peak shock overpressures in the explosive mid-field (see Figure 1, "Late Time") for TNT charges. A comparison of peak pressures measured using piezoelectric transducers (PCB, pencil-type) and using Equation (1) is shown in Figure 5 for the explosive mid-field. For each test, the optical method yields a slightly higher peak pressure. This is presumed to be caused by the mechanical actuation required by the piezoelectric transducer. For the explosive near field measurements described here, Mach numbers higher than approximately 10 require a modification to the Rankine-Hugoiniot formulation shown in Equation (1), necessary because at these higher blast loadings the perfect gas assumption for air is not accurate [11]. Figure 6 shows a comparison of optically- based peak shock pressure measurements for perfect and imperfect gases. At the

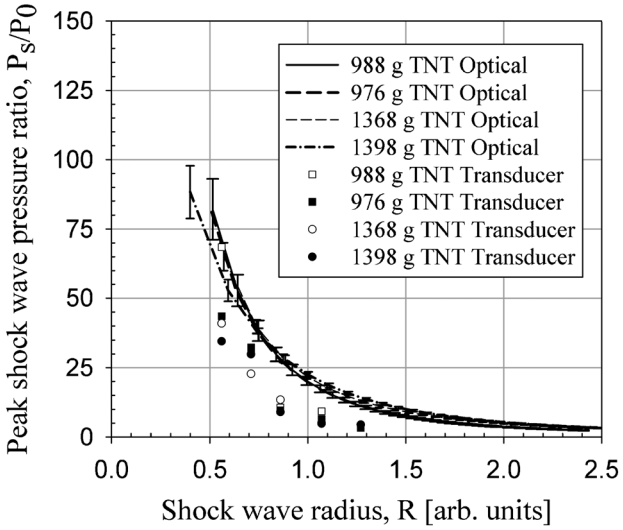

Figure 5. A comparison of optical and mechanical peak shock pressure measurements in the explosive mid-field for several TNT charges.

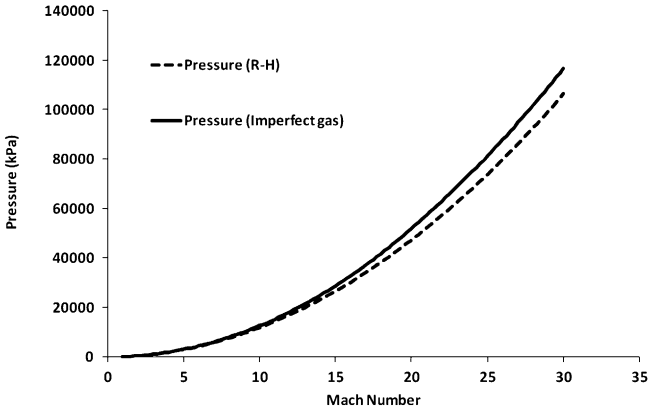

Figure 6. Error in optically-based peak pressure measurements at higher Mach number (higher blast loading) when using the ideal gas assumption in Rankine-Hugoniot theory.

higher Mach numbers encountered for near field measurements, Figure 6 shows error associated with use of Equation (1) may approach 10 %.

4 Experimental

Two different cameras (Cordin Model 570, Photron SA-5) were used to measure shock pressure, depending upon the expected shock velocity. Figures 7 a-c show respectively an overall schematic of the rig used to measure shock velocity, a photograph of a C-4 sphere (450g) positioned within an indoor blast chamber at the US Army Research Laboratory (ARL) facility located at the Aberdeen Proving Ground in MD, and a diagram of the way in which a Photron SA-5 framing camera is used in streak camera mode. The C-4 sphere was center detonated (RP-83 detonator) for each experiment. A mirror positioned above the charge provided a non-direct line of sight for streak camera imaging. For framing camera imaging, a direct line of sight was employed. Figure 7 b) also shows a transducer-equipped blast wall and a blast bar gauge used to measure pressure for these experiments. Results from the blast wall and bar gauge diagnostics are not reported here.

For measurement closest to the charge (highest shock velocity), high speed framing camera images were obtained using a Cordin Co. Model 570 digital framing camera operating at 2.5 Mfps, with an exposure time of 300 ns. Each recorded image was 4 megapixels in size. For each shot, the maximum number of frames was 74. An example of the output from this camera is shown in Figure 3. At distances approaching 1 meter from the charge surface (slower shock velocity), a modified streak camera rig was used. The streak camera rig was somewhat unique in that an addressable digital framing camera (Photron SA-5) was used. By defining the active pixel area to be 8×768 pixels, streak-type images were obtained at 700000 frames per second (fps) at an exposure time of 370 ns. For each shot with this rig the

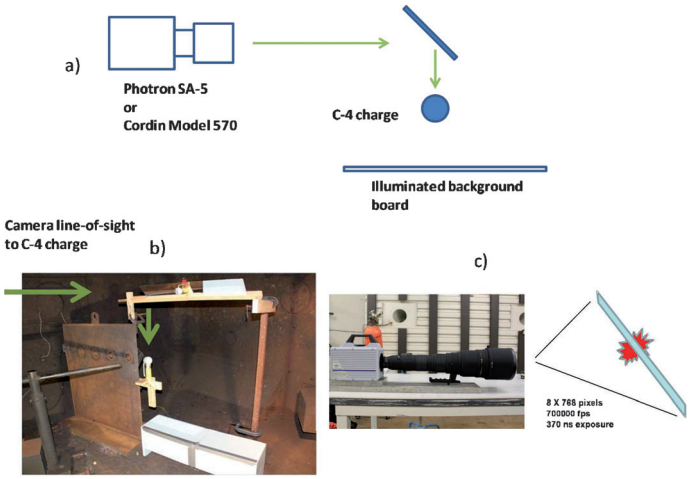

Figure 7. a) A schematic of the rig to measure shock velocity using high speed cameras. b) A 450 g C-4 sphere positioned within an indoor blast chamber at the ARL for one of the tests described here. c) A schematic of the streak camera rig, which employed a Photron SA-5 framing camera with the chip addressed to 8×768 pixels.

maximum number of frames was many thousands, exceeding the number required to image the gases and leading shock within the field of view. Figure 7 c) shows a schematic of this setup. A speckled backing board placed behind the focal plane of the camera provided contrast to enable visualization of the leading edge of the explosive gases and the point at which the leading shock separated from these gases.

The experimental protocol was to use the streak camera rig (Photron SA5) to record images from the charge over the entire explosive near field, and use the faster framing camera (Cordin 570) for measurements of the explosive near field immediately adjacent to the charge, where the gas expansion velocity was highest.

5 Results – Streak Camera Rig

For the streak camera measurements, each record was analyzed using the Photron PFV software. Prior to each shot, a test image was obtained with a meter stick positioned at the focal plane of the camera. From this image, a calibration of millimeters per pixel was obtained, and used in the analysis of the experimental data. In the Photron software, the position of the leading edge of the detonation product gases was given a pixel location, and this location was converted to a distance from charge center in millimeters. Resolution was approximately 1.35 millimeters per pixel. Consecutive images were used to determine distance per unit time, and a peak pressure calculated based upon Mach number from measured shock velocities. Figure 8 shows the result of peak shock pressures calculated using data from the streak camera rig employing a direct numerical differentiation, and results calculated using the blast peak pressure simulator CONWEP [12]. Agreement is reasonable over all, but is poor in regions of high peak pressure/high Mach number. This disagreement at high pressure/Mach number is likely due to the framing rate of the streak camera rig being limited to 700000 fps. For this rig, error in the measurements is believed to be less than 10% at distances greater than approximately 1 charge diameter (about 80 mm), with the main sources of error being the duration of exposure, and deviation from ideal gas behavior at higher Mach number.

In an attempt to minimize the noise inherent in a direct numerical differentiation of the streak data, a third order polynomial was fit to raw distance vs. time data (Figure 9), and the best fit equation was then differentiated to provide a smoother velocity vs. time record. This is shown in Figure 10. As with the results of direct numerical differentiation, the results agree best with CONWEP predictions at peak pressures below about 20000 kPa (approx. 3000 psi).

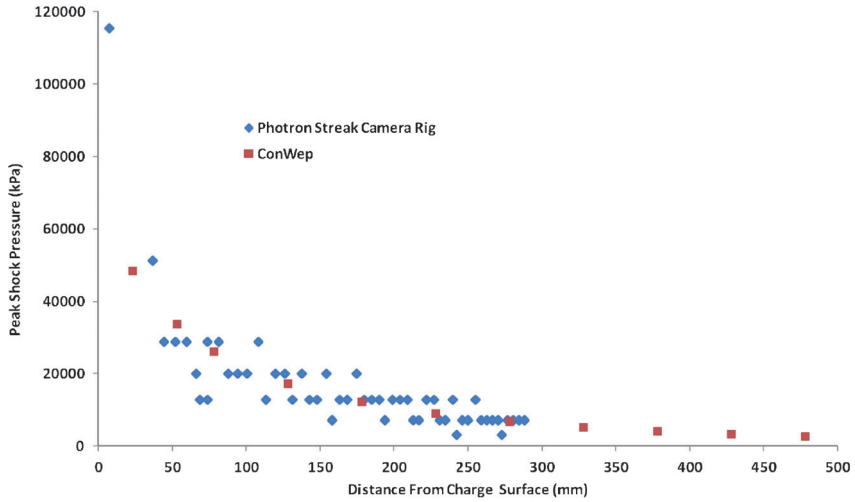

Figure 8. Peak shock pressures calculated using data from the streak camera rig employing a direct numerical differentiation, and results calculated using the blast peak pressure simulator CONWEP.

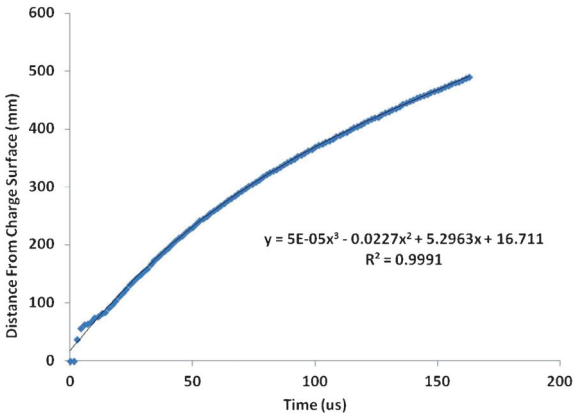

Figure 9. The best fit third order polynomial to a set of streak camera data for 450 g spherical C-4 charges.

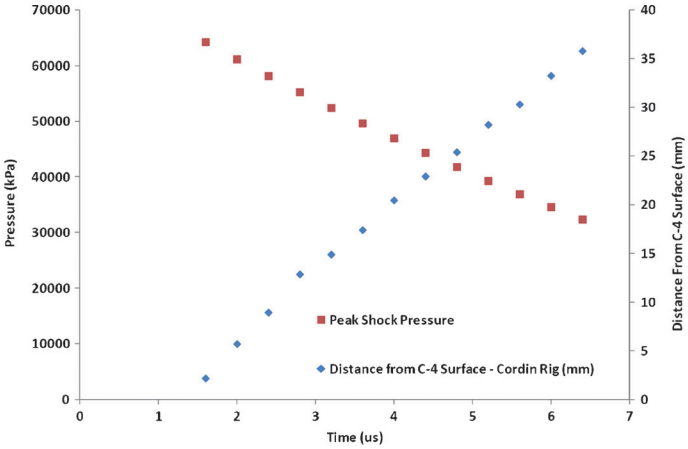

Figure 11. Peak shock pressure and position vs. time for spherical C-4 charges. Measured using the Cordin Model 570 camera.

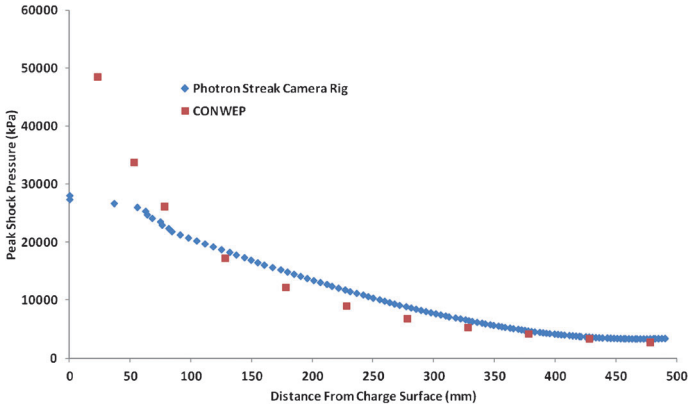

Figure 10. Peak shock pressure based upon the numerical fit to data shown in Figure 9. The disagreement is most severe at pressures above approximately 25000 kPa.

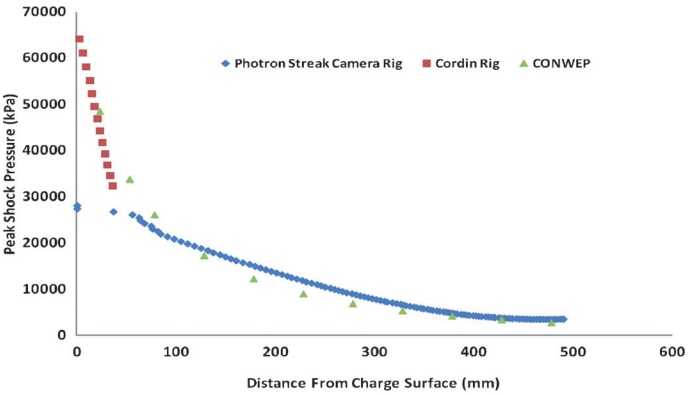

Figure 12. Optically-based peak shock pressure measurements using the framing camera (Cordin Model 570) and the streak camera rig, and predictions based upon CONWEP. Error is believed to be within 10 % of actual, with the largest source of error being the exposure duration of each camera.

6 Results – Framing Camera

Framing camera (Cordin Model 570) images were recorded in a direct line of sight. Consecutive images were analyzed similar to methods employed for the streak camera images, using the Photron PFV software. Figure 11 shows leading shock position and differentiation of a best fit to position data resulting in a peak pressure vs. distance for a C-4 sphere similar to the spheres used in the streak camera measurements. It is worth noting that although the C-4 spheres were prepared using hemispherical molds, the malleable nature of the C-4 caused each sample to vary in sphericity. The line of sight along which the framing camera data was analyzed was chosen to coincide with that used for the streak camera data. Physical limitations of mirror placement prevented the simultaneous use of the two cameras. Figure 11 shows that the higher framing rate of the Cordin camera relative to the streak camera rig (approximately 3.5X) provides data in reasonable agreement to CONWEP at distances immediately adjacent to the charge. Figure 12 shows the results of both measurements of optically-based peak shock pressure and predictions based upon CONWEP. The results overall are in reasonable agreement with CONWEP predictions. Error in the measurements is believed to be less than 10 %, with the main sources of error being the duration of exposure, and deviation from ideal gas behavior at higher Mach number.

7 Summary and Conclusions

The results shown here indicate that high speed, high fidelity imaging (framing rates greater than 1 MegaHertz (MHz) at resolution approaching high definition) can make a significant contribution to analysis of the near field behaviour of high explosives. For extremely high fidelity records, direct numerical differentiation of position vs. time data may be possible, but for noisy data (e.g., Figure 11) a fit to position data, followed by differentiation of the resulting equation, yields smoother data for measurements reported here.

However, fitment of position vs. time data to a physically realistic function (e.g., Friedlander equation [6]) may also be useful, and ultimately more realistic. A real possibility here, and currently under pursuit by us in another test series, is the use of high fidelity imaging to create pressure maps, providing a full cross section of the near field explosive behaviour in a single test. ARL is currently pursuing an extension of this technique to create temperature and chemical species maps in the explosive near field. The fidelity and dimensionality achieved using this method for measuring the peak shock pressure in the near field may be the best tool available for determining performance of new insensitive munitions, and for determining the real utility of fuel additives. Coupling of this technique to techniques that measure surface temperatures of fireballs [8] provides a standoff tool to characterize explosive performance that exceeds present modelling capabilities, and should provide validation data for physical chemical explosives models that incorporate finate rate chemical kinetics.

References

[1] K. L. McNesby, B. E. Homan, R. E. Lottero, *High Brightness Imaging for Real Time Measurement of Shock, Particle, and Combustion Fronts Produced by Enhanced Blast Explosives*, U.S. Army Research Laboratory (ARL), Washington D. C., USA, ARL-TR-3411, January **2005**.

[2] P. W. Cooper, *Explosives Engineering*, Wiley-VCH, Inc., New York, **1996**.

[3] S. Bastea, L. E. Fried, K. R. Glaesmann, W. M. Howard, I. W. Kuo, P. C. Souers, P. A. Vitello, *Cheetah 6.0 Thermochemical Analysis Tool*, Energetic Materials Center Lawrence Livermore National Laboratory, Livermore, CA, USA.

[4] D. C. Sachs, E. Cole, *Air Blast Measurement Technology*, Report Defense Nuclear Agency #DNA 4115F, work performed by Kaman Sciences Corp. (K-76-38U(R), Colorado Springs, CO, USA, September **1976**.

[5] P. L. Waller, *Introduction to Air Blast Measurements*, PCB Tech Note TN-12, www.pcb.com.

[6] C. L. Mader, *Numerical Modeling of Explosives and Propellants*, 3rd Ed.; CRC Press, Boca Raton, FL, USA, **2008**.

[7] K. L. McNesby, B. E. Homan, J. J. Ritter, Z. Quine, R. Z. Ehlers, B. A. McAndrew, Afterburn Ignition Delay and Shock Augmentation In Fuel Rich Solid Explosives, *Propellants Explos. Pyrotech.* **2010**, *35*, 57 – 65.

[8] J. M. Densmore, M. M. Biss, B. E. Homan, K. L. McNesby, Thermal Imaging of Nickel-Aluminum and Aluminum-Polytetrafluoroethylene Impact Initiated Combustion, *J. Appl. Phys.* **2012**, *112*, 084911-084911-5.

[9] J. M. Densmore, M. M. Biss, B. E. Homan, K. L. McNesby, *Evaluation of Reactive-Material-Surrounds Explosive Charges*, U.S. Army Research Laboratory (ARL), Washington D. C., USA, ARL-TR-5603, July **2011**.

[10] G. F. Kinney, K. J. Graham, *Explosive Shocks in Air*, 2nd Edition, Springer-Verlag, Berlin, **1985**.

[11] J. D. Anderson, *Hypersonic and High Temperature Gas Dynamics*, 2nd Edition, AIAA Education, New York, **1996**.

[12] D. Hyde, *User's Guide for Microcomputer Programs: CONWEP and FUNPRO – Applications of TM 5-855-1*, U.S. Army Engineer Waterways Experimental Station, Vicksburg, MS, USA, **1988**.

Received: February 25, 2013
Revised: June 6, 2013
Published online: September 18, 2013

